Collective modes in metals: quantal and semiclassical approaches

2008 J. Phys.: Condens. Matter 20 485219

(http://iopscience.iop.org/0953-8984/20/48/485219)

J. Phys.: Condens. Matter **20** (2008) 485219 (6pp) doi:10.1088/0953-8984/20/48/485219

Collective modes in metals: quantal and semiclassical approaches

J P da Providência

Physics Department, University of Beira Interior, Rua Marquês d'Ávila e Bolama, 6200 Covilhã, Portugal

E-mail: joaodaprovidencia@daad-alumni.de

Received 19 July 2008
Published 28 October 2008
Online at stacks.iop.org/JPhysCM/20/485219

Abstract

A quantal description (da Providência Jr and Barberán 1992 *Phys. Rev.* B **45** 6935–7; Barberán and da Providência Jr 1996 *Z. Phys.* B **101** 3–12) of the collective modes in metals is revisited. Collective variables are explicitly introduced. A time-dependent Slater determinant is assumed for the wavefunction of the system of valence electrons. Analogous models are also investigated using the semiclassical approximation based on the Wigner transform. The results indicate that for those collective modes, which are associated with a large number of particles, namely the cloud of valence electrons, the semiclassical approximation provides good results and is a reliable tool.

1. Introduction

The study of plasmons (collective excitations of the gas of valence electrons in metals) has been a challenging subject [3]. We will be concerned with the energy of plasmons in metals and we will use the quantal and the semiclassical versions of two models [1, 2] describing collective modes of the cloud of valence electrons in metals. In this field there are many experimental results [5–10] which we will try to interpret with our theoretical models.

The semiclassical approximation based on the lowest order of the Wigner–Kirkwood $\hbar$ expansion has been widely used with good results [11]. The idea being that some processes involving a large number of electrons may be explained by classical mechanics provided that it is combined with the Pauli principle. In some cases, the normal modes obtained using the semiclassical approximation compare well with available quantal calculations [4] for the same force parameters. Due to the large number of degrees of freedom, and in order to simplify the calculations, it is often convenient to perform a variational calculation within a restricted space. In [1, 2], two variational calculations of collective modes of the valence electrons in a metal were presented which lead, in one case, to a single branch dispersion relation, and in the other case to a double branch dispersion relation. As a trial wavefunction, a time-dependent Slater determinant of plane waves $|\phi\rangle$ was considered which is related to the Hartree–Fock ground state through a unitary transformation

$$|\phi\rangle = \mathrm{e}^{\mathrm{i}\frac{\hat{S}}{\hbar}}|\phi_0\rangle, \tag{1}$$

where the generator

$$\hat{S} = \sum_{j=1}^{N} S(\mathbf{x}_j, \hat{\mathbf{p}}_j, t) = \sum_{j=1}^{N} \left(Q(\mathbf{x}_j, \hat{\mathbf{p}}_j, t) + P(\mathbf{x}_j, \hat{\mathbf{p}}_j, t)\right), \tag{2}$$

is a Hermitian time-dependent operator, Q is time-even, P is time-odd, $\mathbf{x}_j$ stands for the position of the electron j and $\hat{\mathbf{p}}_j$ is the momentum operator of the electron j ($\hat{\mathbf{p}} = -\mathrm{i}\hbar\nabla$). Following [2] we write $Q = Q_A + Q_B$ and $P = P_A + P_B$, where

$$Q_A(\mathbf{x}, \hat{\mathbf{p}}, t) = 2\alpha \cos(\mathbf{q}\cdot\mathbf{x}), \tag{3}$$

$$Q_B(\mathbf{x}, \hat{\mathbf{p}}, t) = 2\beta\, \hat{\mathbf{p}}\cdot\mathbf{q} \cos(\mathbf{q}\cdot\mathbf{x})\hat{\mathbf{p}}\cdot\mathbf{q}, \tag{4}$$

$$P_A(\mathbf{x}, \hat{\mathbf{p}}, t) = 2\gamma[\hat{\mathbf{p}}\cdot\mathbf{q} \sin(\mathbf{q}\cdot\mathbf{x}) + \sin(\mathbf{q}\cdot\mathbf{x})\hat{\mathbf{p}}\cdot\mathbf{q}], \tag{5}$$

and

$$P_B(\mathbf{x}, \hat{\mathbf{p}}, t) = 2\delta[(\hat{\mathbf{p}}\cdot\mathbf{q})^2 \sin(\mathbf{q}\cdot\mathbf{x})\hat{\mathbf{p}}\cdot\mathbf{q} + \hat{\mathbf{p}}\cdot\mathbf{q} \sin(\mathbf{q}\cdot\mathbf{x})(\hat{\mathbf{p}}\cdot\mathbf{q})^2], \tag{6}$$

with α, β, γ and δ being time-dependent collective variables which describe collective modes of the gas of valence electrons. The dynamics of the system is determined by the quantum mechanical action principle. In the present paper we consider the semiclassical approximation, which means that in

a Wigner–Kirkwood expansion, in powers of $\hbar$, only the lowest order powers are considered. In the classical limit (see the next section for the rules used to obtain the classical limit), the expressions of the Wigner transform of the generators are

$$(Q_A(\mathbf{x}, \hat{\mathbf{p}}, t))_{CL} = 2\alpha \cos(\mathbf{q}\cdot\mathbf{x}), \tag{7}$$

$$(Q_B(\mathbf{x}, \hat{\mathbf{p}}, t))_{CL} = 2\beta\,(\mathbf{p}\cdot\mathbf{q})^2 \cos(\mathbf{q}\cdot\mathbf{x}), \tag{8}$$

$$(P_A(\mathbf{x}, \hat{\mathbf{p}}, t))_{CL} = 4\gamma\mathbf{p}\cdot\mathbf{q}\sin(\mathbf{q}\cdot\mathbf{x}), \tag{9}$$

and

$$(P_B(\mathbf{x}, \hat{\mathbf{p}}, t))_{CL} = 4\delta(\mathbf{p}\cdot\mathbf{q})^3 \sin(\mathbf{q}\cdot\mathbf{x}), \tag{10}$$

where $\mathbf{p} = (\hat{\mathbf{p}})_{CL}$ represents the linear momentum. While in [1], $Q = Q_A$ and $P = P_A$ are considered, so that the trial wavefunction is parametrized by only two collective coordinates α and β, in [2] the truncation scheme $Q = Q_A + Q_B$ and $P = P_A + P_B$ is used, so that the trial wavefunction depends on the collective coordinates α, β, γ and δ. The results we obtain within the semiclassical approximation are compared with experimental data. We find that the semiclassical description reproduces rather well the experimental behavior (eventually doing better than the corresponding quantal models presented in [1, 2]).

2. Method

For small amplitude deviations from the equilibrium state, the quantum mechanical Lagrangian

$$L = \mathrm{i}\hbar\langle\phi|\dot{\phi}\rangle - \langle\phi|H|\phi\rangle, \tag{11}$$

leads to the harmonic Lagrangian,

$$L^{(2)} = \frac{\mathrm{i}}{2\hbar}\langle\phi_0|[\hat{S}, \dot{\hat{S}}]|\phi_0\rangle - \frac{1}{2\hbar^2}\langle\phi_0|[\hat{S}, [H, \hat{S}]]|\phi_0\rangle, \tag{12}$$

which determines the time evolution of the generator $\hat{S}$. The dot over ϕ and S denotes a time derivative. Here H stands for the many-body Hamiltonian,

$$H = \sum_{j=1}^{N}\frac{\hat{\mathbf{p}}_j^2}{2m} + \sum_{i,j}\frac{e^2}{4\pi\epsilon_0|\mathbf{x}_i - \mathbf{x}_j|} + \sum_{j=1}^{N}U(\mathbf{x}_j) + W, \tag{13}$$

where $U(\mathbf{x})$ is the potential energy due to the uniform positive density distribution and W is the electrostatic energy of the positive background.

The classical limit is given by the following rules:

(1) An operator $A(\mathbf{r}, \hat{\mathbf{p}})$ is replaced by its classical limit $A_{CL}(\mathbf{r}, \mathbf{p})$ which is the leading term of the Wigner–Kirkwood expansion of the Wigner transform of $A(\mathbf{r}, \hat{\mathbf{p}})$ in powers of $\hbar$.

(2) The commutator of two operators $[A, B]$ is replaced by $\mathrm{i}\hbar\{A_{CL}, B_{CL}\}$, where the notation $\{,\}$ stands for Poisson brackets

$$\{A, B\} = \sum_{i=1}^{3}\left(\frac{\partial A}{\partial x_i}\frac{\partial B}{\partial p_i} - \frac{\partial A}{\partial p_i}\frac{\partial B}{\partial x_i}\right),$$

where x_i and p_i are respectively the Cartesian coordinates in coordinate and in momentum space.

(3) The expectation value of a one-body operator, $\langle A\rangle = \mathrm{tr}\,\rho A$, is replaced by the integral in phase space $\int \mathrm{d}\Gamma f A_{CL}$ where f is the classical limit of the Wigner transform of the one-body density matrix ρ and $\mathrm{d}\Gamma = 2\frac{\mathrm{d}^3x\mathrm{d}^3p}{(2\pi\hbar)^3}$.

Starting from the Lagrangian (12) and considering the generator $S = Q_A + Q_B + P_A + P_B$ the following semiclassical Lagrangian is obtained:

$$L^{(2)} = \frac{2N}{\pi^2 n_0}\left(\frac{\hbar^4 q^{13}(\delta\dot{\beta} - \beta\dot{\delta})}{7x^7} + \frac{\hbar^2 q^9(\delta\dot{\alpha} - \alpha\dot{\delta} + \gamma\dot{\beta} - \beta\dot{\gamma})}{5x^5} + \frac{q^5(\gamma\dot{\alpha} - \alpha\dot{\gamma})}{3x^3}\right) - T^{(2)}[\alpha, \beta] - E^{(2)}[\gamma, \delta], \tag{14}$$

$$T^{(2)}[\alpha, \beta] = \frac{N}{m\pi^2 n_0}\left(\frac{\hbar^4\beta^2 q^{13}}{7x^7} + \frac{2\hbar^2\alpha\beta q^9}{5x^5} + \frac{\alpha^2 q^5}{3x^3}\right), \tag{15}$$

$$E^{(2)}[\gamma, \delta] = \frac{4N\hbar^2}{m\pi^2 n_0}\left(\frac{\hbar^4\delta^2 q^{17}}{9x^9} + \frac{2\hbar^2\gamma\delta q^{13}}{7x^7} + \frac{\gamma^2 q^9}{5x^5}\right) + \frac{4Nq^2 n_0}{\epsilon_0}\left(\frac{3\hbar^2\delta q^4}{5x^2} + \gamma\right)^2, \tag{16}$$

where $T^{(2)}[\alpha, \beta] = \frac{1}{2\hbar^2}\langle\phi_0|[\hat{Q}, [H, \hat{Q}]]|\phi_0\rangle_{CL}$, $E^{(2)}[\gamma, \delta] = \frac{1}{2\hbar^2}\langle\phi_0|[\hat{P}, [H, \hat{P}]]|\phi_0\rangle_{CL}$ and $x = q/k_{\mathrm{F}}$. From the Lagrangian $L^{(2)}$ a system of four Lagrange equations is obtained. The eigenmode solutions arise assuming the following analytical time-dependency for the collective variables: $\alpha(t) = \alpha_r\cos(\omega_r t)$, $\beta(t) = \beta_r\cos(\omega_r t)$, $\gamma(t) = \gamma_r\sin(\omega_r t)$ and $\delta(t) = \delta_r\sin(\omega_r t)$. Substituting these expressions into the equations of motion, we find a homogeneous system of equations for the amplitudes $\alpha_r, \gamma_r, \beta_r, \delta_r$ which may be expressed as a matrix equation in terms of the vector z_r:

$$(-\omega_r M + H)z_r = 0 \tag{17}$$

where M and H are real and symmetric matrices and $z_r^{\mathrm{T}} = (\alpha_r, \gamma_r, \beta_r, \delta_r)$ represents the transpose of the column vector z_r. We require that the determinant of the homogeneous system of equations is zero, $|-\omega_r M + H| = 0$, in order to have nontrivial solutions. This equation leads to four solutions which are associated with the eigenfrequencies ω_r (appearing in symmetric pairs, $\omega_{-j} = -\omega_j$) and the eigenvectors z_r with $r = -2, -1, 1, 2$. The eigenvectors fulfil an orthogonality relation and may be normalized according to the following orthonormalization relation:

$$z_r^{\mathrm{T}} M z_s = \delta_{rs}\frac{\omega_r}{|\omega_r|}. \tag{18}$$

From the equations of motion it also follows that $\dot{\gamma} = -\frac{\alpha}{2m}$ and $\dot{\delta} = -\frac{\beta}{2m}$. Using the orthonormalization relation, equation (18), we expand, in terms of eigenmodes, the excitation operators $Q_A = 2\cos(\mathbf{q}\cdot\mathbf{x})$ (associated with the vector $z^{\mathrm{T}} = (1, 0, 0, 0)$) and $P_A = 4\mathbf{p}\cdot\mathbf{q}\sin(\mathbf{q}\cdot\mathbf{x})$ (associated with the vector $(z')^{\mathrm{T}} = (0, 1, 0, 0)$). We then have $(1, 0, 0, 0) = \sum_{j=-n}^{n} c_j z_j^{\mathrm{T}}$ and $(0, 1, 0, 0) = \sum_{j=-n}^{n} d_j z_j^{\mathrm{T}}$. It may be seen that

$$\sum_{j=-n}^{n}\hbar\omega_j c_j^2 = \frac{1}{2\hbar^2}\langle\phi_0|[\hat{Q}_A, [H, \hat{Q}_A]]|\phi_0\rangle_{CL}, \tag{19}$$

$$\sum_{j=-n}^{n} \hbar\omega_j\, d_j^2 = \frac{1}{2\hbar^2}\langle\phi_0|[\hat{P}_A,[H,\hat{P}_A]]|\phi_0\rangle_{CL}. \tag{20}$$

with equations (19) and (20) corresponding, respectively, to the linear energy weighted sum rule for the operators $\hat{Q}_A$ and $\hat{P}_A$. The coefficients c_j and d_j are interpreted as transition amplitudes corresponding to the operators $\hat{Q}_A$ and $\hat{P}_A$. Taking into account that $d_j = -c_j m\omega_j$, and since $[H,\hat{Q}_A] = \frac{i\hbar}{2m}\hat{P}_A$, the cubic energy weighted sum rule is obtained:

$$\sum_{j=-n}^{n} \hbar\omega_j^3\, c_j^2 = \frac{1}{2m^2\hbar^2}\langle\phi_0|[\hat{P}_A,[H,\hat{P}_A]]|\phi_0\rangle_{CL}$$
$$= -\frac{2}{\hbar^4}\langle\phi_0|[[H,\hat{Q}_A],[H,[H,\hat{Q}_A]]]|\phi_0\rangle_{CL}. \tag{21}$$

In equations (19)–(21), $n = 1$ if the generator $S = Q_A + P_A$ is considered and $n = 2$ if the generator $S = Q_A + Q_B + P_A + P_B$ is considered. The modes with eigenfrequencies ω_k and ω_{-k} have the same energy $\hbar|\omega_k|$ and exhaust equal fractions of the sum rules.

The Lagrangian given by equation (14) can be directly compared with the Lagrangian given by equation (11) of [2]. One can see that some of the terms appearing in the Lagrangian of [2] do not appear in the semiclassical Lagrangian presented in this note, such as the exchange terms and some terms with their origin in the kinetic energy. In order to be more specific we now consider the simpler scheme of [1] where the trial wavefunction has the generator $\hat{S} = \hat{Q}_A + \hat{P}_A$. In this case the semiclassical harmonic Lagrangian reduces to

$$L^{(2)} = \frac{2N}{3\pi^2x^3n_0}\left(-\frac{6\hbar^2\gamma^2q^9}{5mx^2} - \frac{\alpha^2q^5}{2m} + \gamma\dot{\alpha}q^5 - \alpha\dot{\gamma}q^5\right)$$
$$- \frac{4q^2Nn_0\gamma^2}{\epsilon_0}. \tag{22}$$

In this simpler scheme only the frequencies ω_1 and ω_{-1} result from the Lagrange equations,

$$\omega_1 = -\omega_{-1} = \sqrt{\frac{3\hbar^2k_F^2q^2}{5m^2} + \frac{n_0}{\epsilon_0 m}}, \tag{23}$$

and therefore two of the terms appearing in the expression for the frequency in the equation (21) from [1] are now missing, namely a term due to the exchange contribution and a term which has its origin in the kinetic energy and is proportional to q^4.

3. Numerical results and discussion

We will now present the results obtained from the Lagrangians (22) and (14) and we will compare them with the corresponding quantal results and with the experimental data. In the case of the parametrization $S = Q_A + P_A$ leading to the semiclassical Lagrangian (22) (or to the quantal Lagrangian given by equation (14) in [1]) we will refer to as parametrization I and in the case of the parametrization $S = Q_A + Q_B + P_A + P_B$ leading to the Lagrangian (14) (or to the quantal Lagrangian expressed by equation (11) in [2]) we will refer to as parametrization II. Following [1, 2], and in order to compare with experiment, we will use an effective mass m^* (instead of the bare electron mass m) and a dielectric constant ϵ (instead of the vacuum dielectric constant ϵ_0). The choices for m^*, ϵ and n_0 will depend on the metal considered. In our formalism the linear (LEWSR) and the cubic (CEWSR) energy weighted sum rules are fulfilled. Evaluating the fraction of the sum rules that correspond to each mode, we obtain information concerning the probability of excitation of each mode which will help us to interpret the experimental data.

Due to the analytical expression of the Lagrangian, we are led to frequencies which depend on m^*, ϵ and the equilibrium density n_0 of the valence electrons. The density may be expressed in terms of the parameter r_s such that $n_0 = (4\pi(r_sa_0)^3/3)^{-1}$ where a_0 is the Bohr radius. With parametrization II, two eigenenergies are found for each value of q (we find one eigenenergy with parametrization I). Concerning parametrization II, in the limit when $q \to 0$, one of the eigenenergies is zero and the other one corresponds to the volume bulk plasmon frequency $\omega_p = \sqrt{\frac{n_0}{\epsilon_0 m}}$. Due to our parametrizations of the wavefunction by means of collective coordinates, all the modes derived within these models are collective modes.

For parametrization I, only one branch for the energy is obtained, which implies that for each value of q the corresponding energy exhausts the LEWSR and the CEWSR, thus this case is different from parametrization II. For this reason, for each metal we present two graphs, one with the experimental and theoretical energies corresponding to the parametrizations I and II and a second graph with the fractions of the LEWSR within parametrization II (in the two graphs we always include the quantal and the semiclassical results). In the graphs for the energy and for the fractions of the sum rules, each branch is always associated with a set of symmetric eigenfrequencies (ω_k and ω_{-k}).

With respect to aluminum we have considered the values $m^* = 1.05\,m$ and $\epsilon = 1.05\,\epsilon_0$ which were obtained from the calculated shifts of the plasmon energies at $q = 0$ due to inhomogeneity and core polarization effects [12]. The experimental data is taken from [5]. In figure 1 we present results for aluminum. On the higher graph we present the energies of the eigenmodes as a function of q^2 and on the lower graph we present the fractions of the LEWSR corresponding to the eigenenergies obtained within parametrization II. In the upper graph, the dotted curve is the result obtained within parametrization I in the semiclassical approximation while the dash–dotted curve is the corresponding quantal result obtained within parametrization I [1]. The two dashed curves appearing in both graphs refer to the eigenmodes obtained doing the quantal calculation in parametrization II [2], and the two continuous curves are the results obtained in the semiclassical approximation with parametrization II. We see that the semiclassical result within parametrization I has a reasonable behavior between the experimental points and also that the thin continuous curve corresponding to the higher mode in parametrization II (semiclassical approximation) shows a behavior close to the experimental points. With respect to the quantal results the dash–dotted curve (parametrization I) agrees well with the experimental data for lower values of

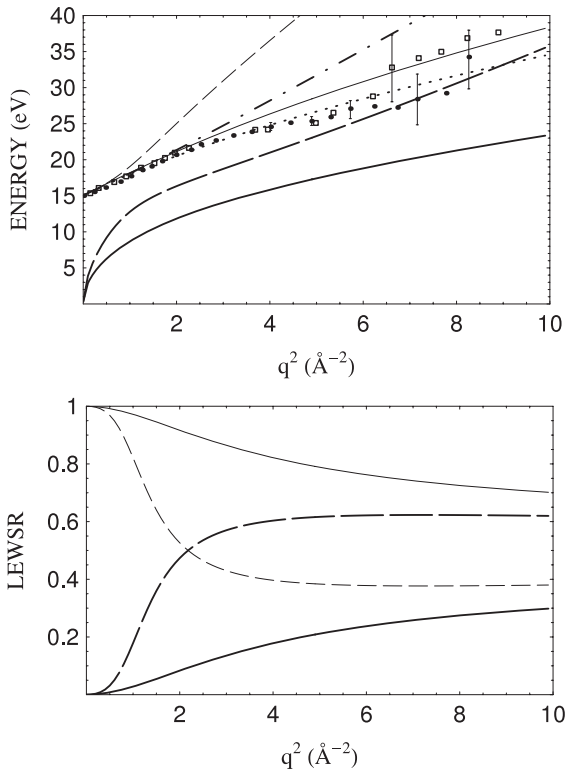

Figure 1. Numerical results for aluminum ($r_s = 2.07$, $m^* = 1.05\,m$ and $\epsilon = 1.05\,\epsilon_0$). The curves of the above graphs represent the quantal and the semiclassical results obtained within the models of [1, 2]. In the upper graph, the excitation energies of the collective modes are plotted as a function of the wavevector q and the experimental data is taken from [5]. The dotted curve (semiclassical result) and the dash–dotted curve (quantal result) correspond to the eigenenergy obtained in the simpler model [1] where the generator S is approximated by a polynomial of degree 1 in the momentum operator (parametrization I). This model leads to just one eigenenergy for each value of q. Two eigenenergies are obtained assuming a polynomial of degree 3 in the momentum operator for the generator S (parametrization II) [2] and are represented in both graphs by the continuous curves (semiclassical result) and by the dashed curves (quantal result). In order to make judgements about the excitation probability of these collective modes we plot, on the lower graph, the fractions of the LEWSR corresponding to the eigenenergies obtained, assuming for the generator S a polynomial of degree 3.

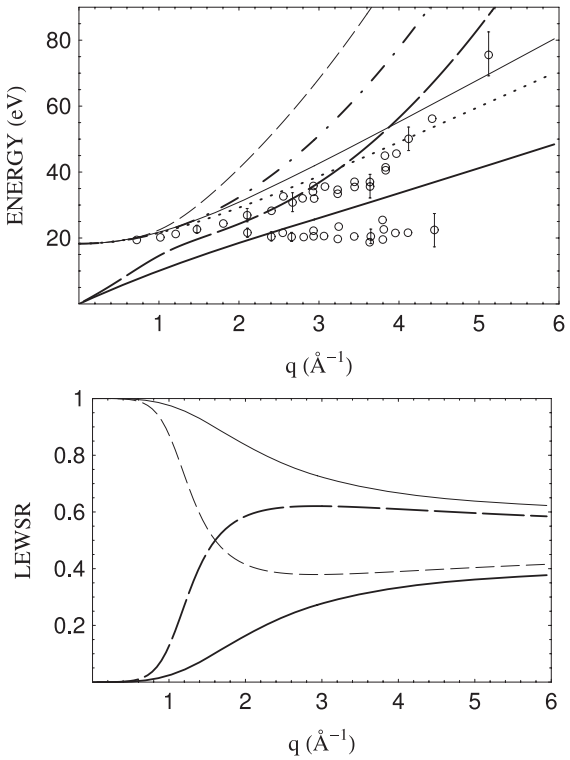

Figure 2. Numerical results for beryllium ($r_s = 1.88$, $m^* = m$ and $\epsilon = \epsilon_0$).

q, but the agreement becomes worse for higher values of q. Within parametrization II we see that for lower values of q the quantal result corresponding to the higher mode (thin dashed curve) is closer to the experimental results, while for higher values of q the quantal lower mode (thick dashed curve) gets closer to the experimental results. These behaviors are directly related with the fractions of the LEWSR presented in figure 1 on the lower graph: while in the semiclassical case the mode with the higher energy (thin continuous curve) exhausts always more than 50% of the LEWSR and has an energy closer to the experimental results, in the case of the quantal calculation the situation changes and we see that for values of q^2 larger than 2.2 Å^{-2}, the lower mode (thick dashed curve) exhausts more than 50% of the LEWSR and gets closer to the experimental results.

The experimental data considered for beryllium is taken from [6]. For beryllium (see figure 2) we have used $m^* = m$ and $\epsilon = \epsilon_0$. Within parametrization II, when we look at the experimental results, it is clear that the semiclassical results (continuous curves) follow the experimental data better than the quantal results [2] (dashed curves). The same can be said with respect to parametrization I, since the semiclassical result, represented by the dotted curve, is closer to the experimental data than the quantal result given by the dash–dotted curve. With respect to the quantal result (dashed curves), for q larger than 1.68 Å^{-1} the branch with lower energy exhausts more than 50% of the LEWSR and it is also clear from figure 2 that in this region the lower branch agrees better with the experimental results than the higher branch, which deviates strongly in direction with higher values of the energy.

The experimental data in figure 3 refers to sodium and is obtained from electron-energy-loss spectroscopy in [7]. We use an effective mass $m^* = 1.05\,m$, also taken from [7], and the value $\epsilon = 1.05\,\epsilon_0$ was adjusted so that the volume plasmon agrees for $q = 0$ with the experimental result. The dotted curve (semiclassical approximation-parametrization I) and the thin continuous curve have a good agreement with the experimental data. The dash–dotted curve (parametrization I-quantal calculation) also shows a good agreement with the experimental results. We note that on the lower graph the thin continuous curve exhausts most of the LEWSR (92% for $q = 1$ Å^{-1}). With respect to the quantal result concerning parametrization II, for low values of q there is a good agreement between the higher mode (thin dashed curve) and the experimental results and for higher values of q the

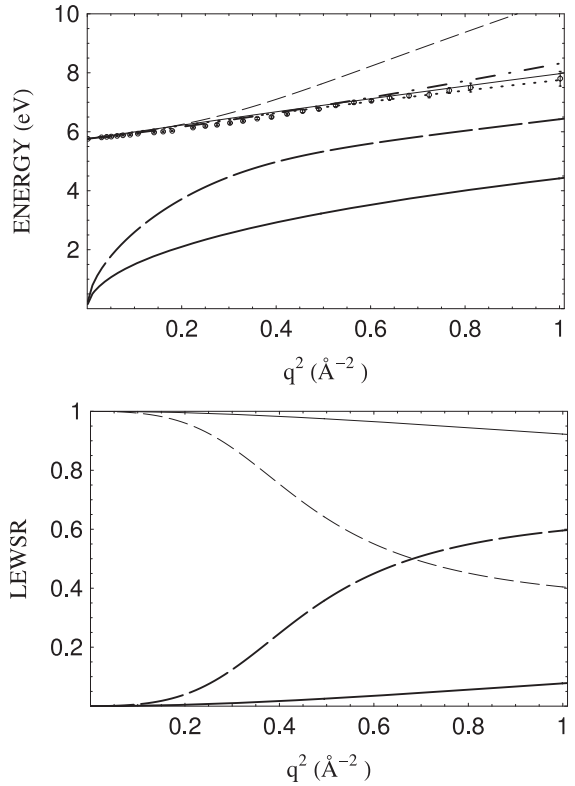

Figure 3. Numerical results for sodium ($r_s = 3.93$, $m^* = 1.05\,m$ and $\epsilon = 1.05\,\epsilon_0$).

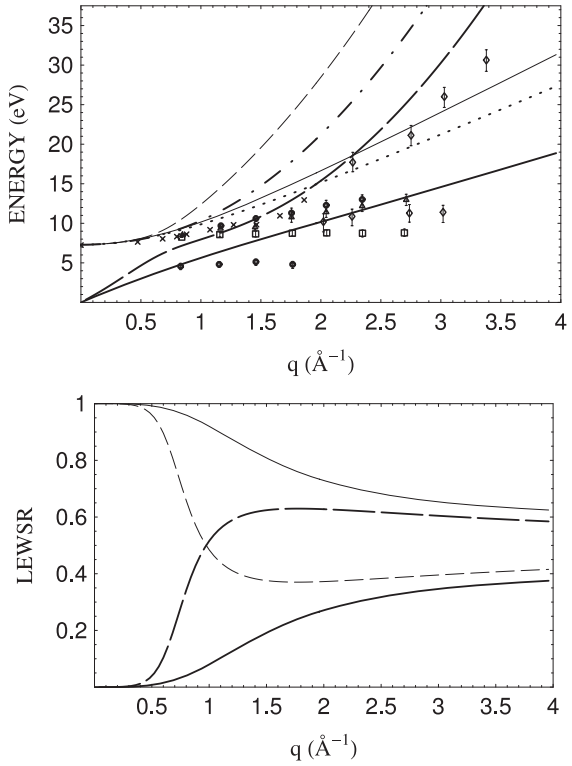

Figure 4. Numerical results for lithium ($r_s = 3.22$, $m^* = m$ and $\epsilon = 1.25\,\epsilon_0$).

experimental results actually lie between the two branches (dashed curves). In fact for $q = 1$ Å^{-1} the experimental data lie closer to the lower branch than to the higher branch and this is in agreement with the fact that here the fraction of the LEWSR exhausted by the mode with lower energy is greater than 50% for q larger than 0.686 Å^{-1}.

We finally consider the case of lithium ($r_s = 3.22$) presented in figure 4 for which (as for beryllium and aluminum) the experimental data indicates more than one energy branch. The experimental data is taken from [8] (diamonds), [9] (squares, triangles and circles), and [10] (×). We have used $m^* = m$ and $\epsilon = 1.25\,\epsilon_0$. We see that many of the experimental values shown in the upper graph of figure 4 do not even lie between the two dashed curves referring to the quantal calculation associated with parametrization II. In this case we have agreement of the experimental data with the higher energy eigenmode for small values of q up to 0.5 Å^{-1}. When we consider parametrization I we observe that the dotted curve (semiclassical calculation) has a better agreement with the experimental data than the dash–dotted curve (quantal calculation, parametrization I). The two semiclassical branches obtained with parametrization II (continuous curves) show a reasonable agreement with the experimental data presented and we observe that the exhausted fractions of the LEWSR behave accordingly, since for q equal to 2.28 Å^{-1} the lower energy branch already exhausts more than 30% of the LEWSR which we associate with the fact that more than one branch is observed experimentally. With respect to the quantal results the branch with lower energy exhausts more than 50% of the LEWSR for $q > 1$ Å^{-1}.

As a remark, we observe that the present semiclassical model (parametrization II) corresponds to more general generators than the ones chosen in [2]. In fact there is an infinity of operators $\overline{Q}_B$ and $\overline{P}_B$ for which the semiclassical limit is given by equations (8) and (10), namely:

$$\overline{Q}_B(\mathbf{x},\mathbf{p},t) = 2\beta\left[\mu_1\hat{\mathbf{p}}\cdot\mathbf{q}\cos(\mathbf{q}\cdot\mathbf{x})\hat{\mathbf{p}}\cdot\mathbf{q} + \frac{\mu_2}{2}\left((\hat{\mathbf{p}}\cdot\mathbf{q})^2\cos(\mathbf{q}\cdot\mathbf{x}) + \cos(\mathbf{q}\cdot\mathbf{x})(\hat{\mathbf{p}}\cdot\mathbf{q})^2\right)\right], \tag{24}$$

and

$$\overline{P}_B(\mathbf{x},\mathbf{p},t) = 2\delta\left[\nu_1\left((\hat{\mathbf{p}}\cdot\mathbf{q})^2\sin(\mathbf{q}\cdot\mathbf{x})\hat{\mathbf{p}}\cdot\mathbf{q} + \hat{\mathbf{p}}\cdot\mathbf{q}\sin(\mathbf{q}\cdot\mathbf{x})(\hat{\mathbf{p}}\cdot\mathbf{q})^2\right) + \nu_2\left((\hat{\mathbf{p}}\cdot\mathbf{q})^3\sin(\mathbf{q}\cdot\mathbf{x}) + \sin(\mathbf{q}\cdot\mathbf{x})(\hat{\mathbf{p}}\cdot\mathbf{q})^3\right)\right], \tag{25}$$

where $\mu_1 + \mu_2 = \nu_1 + \nu_2 = 1$.

4. Conclusion

We have presented numerical results for the plasmon excitation energies in different metals which we have compared with the experimental data and we have investigated the excitation probabilities by means of the linear and cubic energy weighted sum rules.

As expected, the semiclassical expressions do not involve the analogues to some contributions which appear in the quantal expressions (for example the exchange terms). It is therefore remarkable that the performance of the semiclassical

approach is comparable, and in some cases superior, to the corresponding quantal approach, as for instance with respect to interpretation of experimental results related to processes involving large momentum transfer.

In the present note we give the expression of a Lagrangian from which one can easily derive the eigenfrequencies as well as the fractions of the linear and the cubic energy weighted sum rules corresponding to each eigenmode. We therefore believe that this might be a helpful tool in carrying out spectroscopic studies.

References

[1] da Providência J Jr and Barberán N 1992 *Phys. Rev.* B **45** 6935–7

[2] Barberán N and da Providência J Jr 1996 *Z. Phys.* B **101** 3–12

[3] Raether H 1980 *Excitation of Plasmons and Interband Transitions by Electrons* (*Springer Tracts in Modern Physics* vol 88) (Berlin: Springer)

[4] Andō K and Nishizaki S 1982 *Prog. Theor. Phys.* **68** 1196

[5] Batson P E, Chen C H and Silcox J 1976 *Phys. Rev. Lett.* **37** 937

[6] Vradis A and Priftis G D 1985 *Phys. Rev.* B **32** 3556

[7] vom Felde A, Sprosser-Prou J and Fink J 1989 *Phys. Rev.* B **40** 10181

[8] Priftis G D, Boviatsis J and Vradis A 1978 *Phys. Lett.* A **68** 482

[9] Schülke W, Nagasawa H, Mourikis S and Lanzki P 1986 *Phys. Rev.* B **33** 6744

[10] Eisenberger P, Platzman P M and Schmidt P 1975 *Phys. Rev. Lett.* **34** 18

[11] Ring P and Schuck P 1980 *The Nuclear Many-Body Problem* (Berlin: Springer)

[12] Sturm K 1978 *Z. Phys.* B **29** 27